Evaporation of Three-Dimensional Wavy Liquid Film Entrained by Turbulent Gas Flow

Inoue, Takuya
Department of Aeronautics and Astronautics, Kyushu University : Graduate Student

Inoue, Chihiro
Department of Aeronautics and Astronautics, Kyushu University : Associate Professor

Fujii, Go
Aerospace Research and Development Directorate, Research Unit II, Japan Aerospace Exploration Agency : Researcher

Daimon, Yu
Aerospace Research and Development Directorate, Research Unit III, Japan Aerospace Exploration Agency : Senior Researcher

出版情報：AIAA Journal. 60 (6), pp.3805-3812, 2022-02-02. American Institute of Aeronautics and Astronautics
バージョン：
権利関係：

Evaporation of Three-Dimensional Wavy Liquid Film Entrained by Turbulent Gas Flow

Takuya Inoue* and Chihiro Inoue†
Kyushu University, Fukuoka, 819-0395, Japan

Go Fujii‡ and Yu Daimon§
Japan Aerospace Exploration Agency, Tsukuba, Ibaraki, 305-8505, Japan

A film cooling technique using a liquid film subjected to a hot gas flow in a turbulent condition is theoretically investigated. We successfully incorporate the two essential factors for the evaporating liquid film, droplet entrainment and three-dimensional film architecture, allowing for the physically-consistent straightforward formulation. The validity of the present model is convinced by reproducing combustion test results conducted for two types flight-model bipropellant thrusters, in which the film length or dryout point shortens approximately inversely proportional to the combustion pressure. The underlying scenario to determine the film length is revealed. The gas flow initiates the originally smooth liquid film to be destabilized by Kelvin-Helmholtz instability in the axial direction and accelerates the wave crests leading to Rayleigh-Taylor instability in the transverse direction. Superposing the two types of waves produces three-dimensional cusps on the film as roots of entrained droplets. The convective heat transfer evaporating the liquid film is enhanced by the entrainment, reducing the net film flow rate, and by the cusp structure, enlarging the area of liquid/gas interface along the transverse direction in particular.

Nomenclature

a = wave amplitude [m]

b = plate width [m]

D = pipe diameter [m]

f = friction factor

h = thickness of liquid film [m]

h_g = heat transfer coefficient [W/m^2·K]

*Graduate student, Department of Aeronautics and Astronautics, 744 Motooka, Nishi-ku.
†Associate Professor, Department of Aeronautics and Astronautics, 744 Motooka, Nishi-ku, AIAA Member.
‡Researcher, Aerospace Research and Development Directorate, Research Unit II, 2-1-1 Sengen, AIAA Member.
§Senior Researcher, Aerospace Research and Development Directorate, Research Unit III, 2-1-1 Sengen, AIAA Member.

L = characteristic length [m]

M_R = mixture ratio (flow rate ratio of oxidizer to fuel)

P_c = combustion pressure [Pa]

Q = volume flow rate of liquid film [m^3/s]

T = temperature [K]

u = velocity [m/s]

u_c = phase velocity of roll wave [m/s]

u_m = mean velocity of liquid film [m/s]

U = characteristic velocity [m/s]

x = axial direction or measurement point [m]

χ = area expansion factor

δ = vorticity thickness of gas stream [m]

ΔH = latent heat [J/kg]

Φ = film length [m]

λ = wavelength in the axial direction [m]

λ_p = wavelength in the transverse direction [m]

ρ = density [kg/m^3]

σ = surface tension coefficient [N/m]

τ = shear stress [Pa]

η = coefficient of viscosity [Pa·s]

ξ = entrainment rate

Subscripts

c = combustion gas

d = droplet

g = gas

l = liquid

s = saturation

I. Introduction

DYNAMICS of a thin liquid film extending on a wall exposed to a fast gas flow is a general thermo-fluid issue in many practical situations, such as film-cooling technology[1–3], icing on aircraft wings[4–6], and drying of paints and cleaning solutions[7]. Past and recent studies including quantitative measurements [5, 8–15] provide a scenario that the

turbulent gas flows over the initially smooth film, soon drives the film with complex wavy structures by Kelvin-Helmholtz (KH) instability as a roll wave, accelerates the wave crests producing transverse wave by Rayleigh-Taylor (RT) instability as a ripple wave, stretches ligaments, and eventually entrains droplets disintegrated by Plateau-Rayleigh instability, all in a sequential fashion. The waves intricately merge and break downstream[10, 16] being a disturbance wave[5, 13, 17, 18] with large amplitude. The waviness of liquid film can directly enhance heat/mass transfer across the liquid/gas interface. Additionally, the droplet entrainment significantly reduces the net film flow rate and may cause mechanical erosion downstream as well[13].

For a liquid rocket engine combustion chamber employing the film cooling technique[1, 2, 7, 19, 20], minimizing the coolant flow rate is desired to improve the performance of characteristic velocity and specific impulse[3, 19, 21] with achieving the sufficient heat resistance. Liquid fuel jets are often ejected on the inner surface of the combustion chamber in a bipropellant thruster below the critical pressure of propellants, followed by the propagating liquid film covering the wall. In the past, Kinney et al.[22] intensively took snapshots of annular film flow, clearly convincing the wavy film being destabilized by the shearing concurrent gas stream. Experimental studies inside rocket engine combustion chambers have been conducted[23, 24], as well as analytical/numerical investigations[25–28] for the prediction of liquid film length, corresponding to the axial length of liquid film until it completes evaporation at dryout point as an important thermal parameter to determine the film cooling rate and to design the injectors for the film coolant. Recently, Fujii et al.[3] succeeded in high-speed imaging for the unsteady wavy film dynamics inside a practical 10N-class bipropellant thruster under a combustion condition, quantifying the film velocity of $1\mathrm{m/s}$ and thickness of $10\mu\mathrm{m}$. A recent review article by Shine and Nidhi[1] emphasizes that current prediction models for the liquid film length lack the effect of entrainment in particular and still contain many empirical correlations, resulting in the limited applicability. Moreover, the wavy film structure is three-dimensional (3D) in nature, while 3D analyses for the evaporating thin liquid film can be rarely found. The development of a physical model for the evaporating coolant film is recognized still under progress[29].

In the present study, we originally develop a physically-consistent theoretical model for the evaporating film by further extending the latest comprehensive model for non-evaporative liquid film dynamics, established by the authors[15]. To the best of our knowledge, this paper firstly successfully incorporates the 3D wavy structure of the evaporating liquid film, enhancing heat transfer, and the entrainment effect, reducing net film flow rate, deduced as a general formulation. As a result, the present study not only contributes to the quantitative prediction for the film length inside rocket engines, but it also enriches a fundamental understanding of physics underlying the evaporating liquid film sheared by a turbulent gas flow as an essential phenomenon. In the following, the new model is derived at every intermediate step in Section III. In Section IV, we demonstrate the validity of the present model through a comparison with several experimental results including combustion tests recently conducted for practical bipropellant thrusters, and discuss the 3D unsteady dynamics of evaporating liquid film. Conclusions are finally summarized in Section V.

II. Modeling

Figure 1 schematically illustrates that the gas flows with main velocity u_g and vorticity thickness δ, and the liquid film proceeds with mean velocity u_m and thickness h on the wall. The roll wave develops with wavelength of λ and amplitude of a. The wavelength of ripple wave is depicted as λ_p. We derive the film flow in a pipe with diameter of D or on a plate with width of b in a consistent expression. The time-averaged volume flow rate of liquid is given as

$$Q = \pi D h u_m \quad \text{in the pipe,} \tag{1}$$

$$Q = b h u_m \quad \text{on the plate.} \tag{2}$$

Shear stress of the turbulent gas flow acting on the interface is established by introducing friction factor of f.[30–32]

$$\tau = \frac{1}{2} f \rho_g u_g^2 \tag{3}$$

Couette flow is reasonably assumed for the film[8, 33], in which the velocity equals to zero on the wall and $2u_m$ at the liquid/gas interface with a linear profile. The balance of shear stress across the interface is deduced.

$$\eta_l \frac{2u_m}{h} = \tau \tag{4}$$

From Eqs. (1)-(4), we obtain time-averaged liquid velocity and thickness as a function of the gas Reynolds number

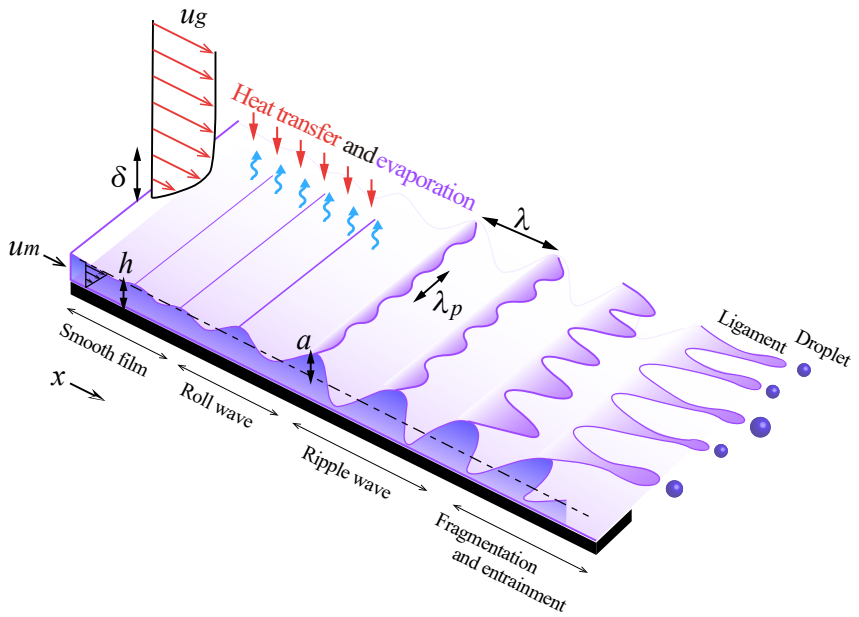

Fig. 1 Evaporating liquid film dynamics subjected to turbulent gas stream.

$Re_g = \rho_g u_g L/\eta_g$ and liquid film Reynolds number $Re_l = \rho_l u_m h/\eta_l$, respectively. Normalization is done by using the characteristic length L and velocity U, such that $L = D$ and $U = Q/(\pi D^2)$ for the pipe flow, and $L = x$ and $U = Q/(bx)$ for the flow on a plate.

$$\frac{u_m}{U} = \frac{\sqrt{f}}{2}\frac{\eta_g}{\eta_l}\sqrt{\frac{\rho_l}{\rho_g}}Re_l^{-1/2}Re_g \tag{5}$$

$$\frac{h}{L} = \frac{2}{\sqrt{f}}\frac{\eta_l}{\eta_g}\sqrt{\frac{\rho_g}{\rho_l}}Re_l^{1/2}Re_g^{-1} \tag{6}$$

The gas stream has a continuous velocity profile with non-zero boundary layer above the interface (see Fig. 1), represented by vorticity thickness δ equivalent with $\eta_g u_g/\tau$, given as follows[32].

$$\frac{\delta}{L} = \frac{2}{f}Re_g^{-1}. \tag{7}$$

The large velocity difference $u_g/u_l \gg 1$ induces KH instability, stimulated by the inflectional point created inside the boundary layer[34, 35]. For the KH instability accompanying finite-thickness vorticity layer, δ is a characteristic length scale[9], providing wavelength of the roll wave independent of capillarity.

$$\lambda \approx \delta\sqrt{\frac{\rho_l}{\rho_g}} \tag{8}$$

The roll wave propagates downstream with phase velocity[36]

$$u_c = \frac{u_m\sqrt{\rho_l} + u_g\sqrt{\rho_g}}{\sqrt{\rho_l} + \sqrt{\rho_g}}. \tag{9}$$

The gas friction superior to the stabilizing force of surface tension as $\tau \geq \sigma/\lambda$ allows the amplitude of the roll wave to grow to the order of film thickness as $a \approx h$[5]. Then, the gas progressively accelerates the heavy wave crests toward a much lighter gas phase, leading to RT instability[37, 38]. As the result, the regularly lined roll wave is strongly corrugated into the transverse direction being ripple wave. The wavelength of λ_p is given as follows[9].

$$\lambda_p = \delta We_\delta^{-1/3}(\frac{\rho_g}{\rho_l})^{-1/3} \tag{10}$$

Here, the Weber number is of $We_\delta = \rho_g u_g^2\delta/\sigma$ based on the length scale of δ. The amplitude of the ripple wave enlarges, creating a cusp by the superposition of roll wave and ripple wave as in Fig. 2(a). Since the cusp is the origin of a ligament producing droplets downstream, the cusp volume approximately coincides with total droplet volume detaching from the cusp. We derive $\lambda_p < \lambda$ as discussed later, thus, the cross-sectional area of the conical cusp corresponds to λ_p^2 and the height is a equivalent to h. The volume of a single cusp is estimated to be approximately $\lambda_p^2 h$. As shown in Fig. 2(b),

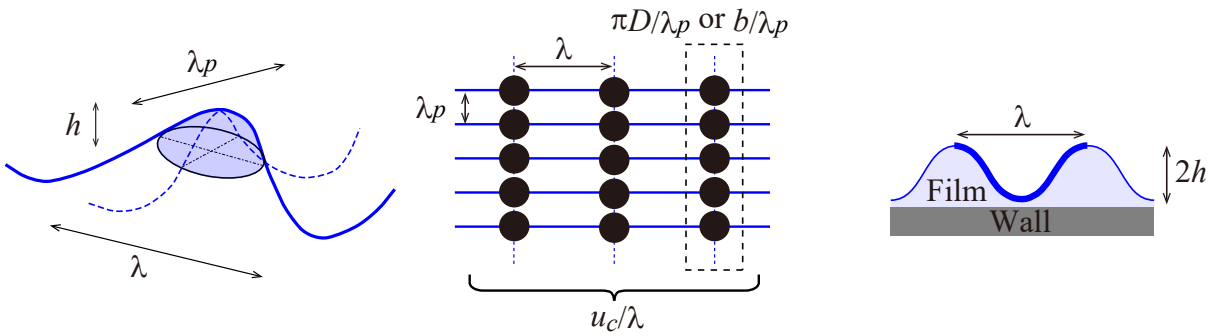

(a) Single cusp. (b) Cusp number. (c) Cross-section of cusps.

Fig. 2 3D cusp model on wavy liquid film.
(b) Top view. The closed circles indicate cusps, arranged in the axial and transverse directions. (c) Length along the wavy film depicted by the blue bold line. χ_a corresponds to the ratio of the length against λ. The same idea is applicable to the transverse direction.

the number of cusps created is $\pi D/\lambda_p$ along the circumference of pipe or b/λ_p across the plate width, propagating with the rate of $(\lambda/u_c)^{-1}$ along the axial direction. The product of cusp volume and all cusp numbers passing in unit time provides the entrained volume flow rate Q_d. The entrainment rate, $\xi(= Q_d/Q)$, is eventually formulated by wavelength ratio and velocity ratio.

$$\xi \approx \frac{\lambda_p}{\lambda}\frac{u_c}{u_m} \tag{11}$$

The entrained film flow doesn't contribute to the film coolant, deteriorating the cooling performance by reducing the net film flow rate[1].

The 3D wavy film structure directly expands the liquid/gas wetting area compared to a flat film surface. A simple model illustrated in Fig. 2(c) suggests that the area expansion rate of wavy film against smooth film in a unit wavelength is approximately estimated as $\chi_a \approx 2\sqrt{(\lambda/2)^2 + (2h)^2}/\lambda = \sqrt{1 + (4h/\lambda)^2}$ in the axial direction, and $\chi_p = \sqrt{1 + (4h/\lambda_p)^2}$ in the transverse direction. The wavy film has a larger wetting area of factor

$$\chi = \chi_a \chi_p, \tag{12}$$

which is larger than unity.

Now let us solve the heat transfer problem in a pipe. Inside a combustion chamber, a liquid film temperature on a wall promptly becomes the saturation temperature T_s as convinced by Fujii et al.[3] The wall temperature within the area covered by the liquid film is approximately equal to T_s[39]. We treat the wall as adiabatic condition and consider a heat source of convective heat transfer from the turbulent hot gas. The temperature gap between the hot gas and liquid film is given by $(T_c - T_s)$. The convective heat transfer coefficient h_g is formulated by the well-known *Bartz* equation[40],

following $h_g \propto P_c^{0.8}$, as well as Dittus-Boelter equation[41, 42]. The heat balance between the heat convection and the latent heat deduces the film length Φ. The present new model implements the entrainment, reducing the film flow rate to be $Q(1-\xi)$, and the wavy film, enriching the heat transfer area multiplied by the factor χ, leading to the original formulation at last.

$$\Phi = \frac{\rho_l Q \Delta H}{\pi D h_g (T_c - T_s)} \frac{1-\xi}{\chi} \tag{13}$$

The conventional model doesn't consider the entrainment nor the film waviness, corresponding with $\xi = 0$ and $\chi = 1$. The liquid film eventually fully vaporizes and self-decomposes, contributing to the chamber pressure and performance[21, 43].

III. Results and Discussion

Firstly, a non-evaporative liquid film is investigated inside a pipe and on a plate for validating the model of 3D film structure and entrainment. Then, an evaporating liquid film inside a circular combustion chamber of bipropellant thruster is discussed.

A. Non-Evaporating Film

Table 1 shows the two types of analysis conditions, corresponding with the recent experiments for pipe flow[14] and flow on flat plate[5]. The distinct working liquid is ethanol and water, subjected to the fast air stream. Applied friction factors are $f = 0.080 Re_g^{-1/4}$[30, 31] and $f = 0.07$[44] for the pipe flow and plate flow, respectively. Figure 3 presents time-averaged experimental results of film velocity and thickness plotted along the vertical axis, compared with analytical results in the horizontal axis derived from Eqs. (5)(6). The analytical results of normalized mean velocity and film thickness under variation of gas velocity are well equivalent with the corresponding experimental

Table 1 Cold-flow test conditions

Flow type	Pipe[14]	Plate[5]
Gas/Liquid	Air/Ethanol	Air/Water
Size[mm]	D=10	b=130
x[mm]	20	250
Re_g	$\leq 1.6\times10^5$	$\leq 3.0\times10^5$
Re_l	≤ 10	≤ 150
ρ_g[kg/m^3]	≤ 1.2	1.2
η_g[μPa·s]	19	19
ρ_l[kg/m^3]	790	1000
η_l[mPa·s]	1.2	1.0
σ[mN/m]	23	73

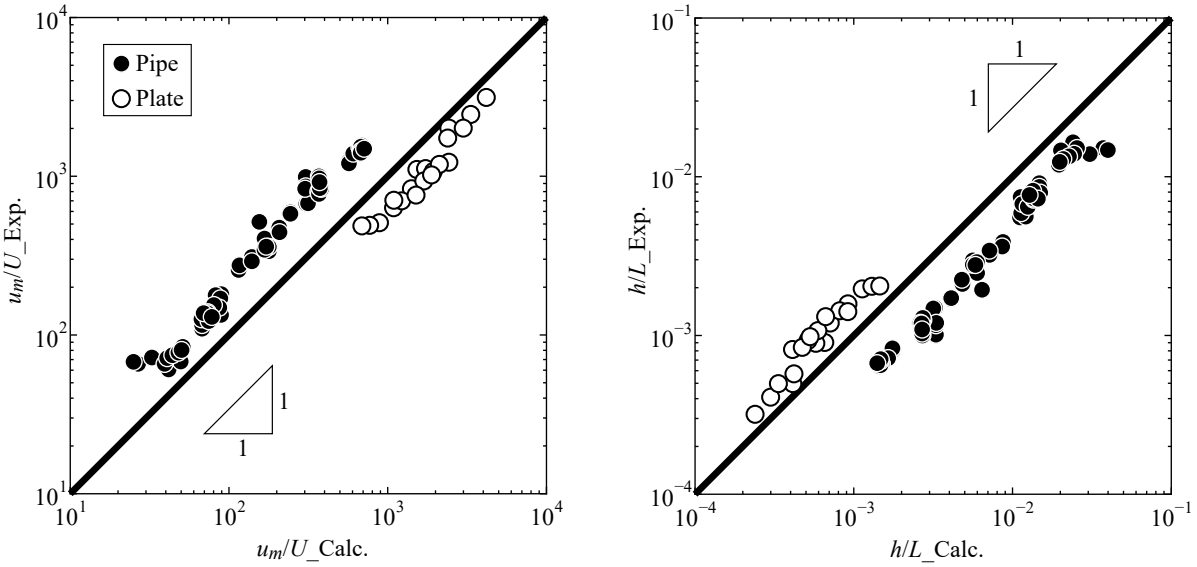

(a) Normalized film velocity.

(b) Normalized film thickness.

Fig. 3 Experimental and calculated results of film velocity and thickness.

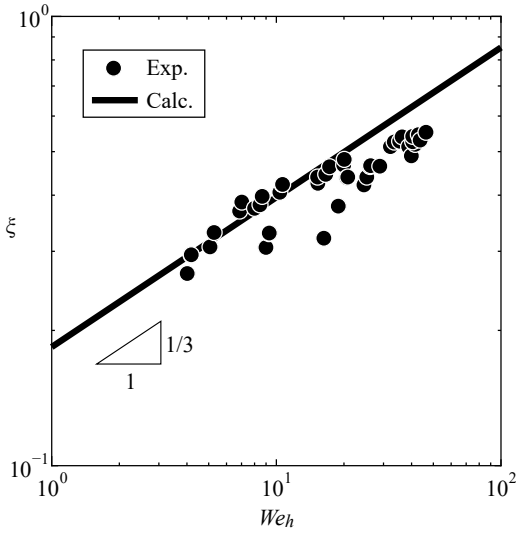

Fig. 4 Entrainment ratio.
The gas velocity is fixed as $u_g = 320\mathrm{m/s}$, while the gas density is varied in a vacuum chamber[14]. The liquid conditions are constant.

results for the pipe flow and plate flow, across the three orders of magnitude. Hence, Eqs. (5)(6) are valid as the formulation of time-averaged film characters for both flow types in the unified expressions. The systematic deviation is caused by the difference in friction factor between the present model and the experiments. Throughout the analysis conditions, the liquid film is promptly covered by a velocity boundary layer forming the Couette flow driven by the shearing gas, consistent with the viscous timescale $h^2/(\eta_l/\rho_l)$ being always smaller than advection time of x/u_m, or say $Re_l < x/h \sim L/h$ as confirmed in Fig. 3(b).

Figure 4 presents the experimental results of entrainment rate[14] with the analytical result as a function of film Weber number, $We_h = \rho_g u_g^2 h/\sigma$. The result calculated by Eq. (11) reproduces well the experimental results in a quantitative sense, showing the monotonic trend that the entrainment rate increases as the gas momentum $\propto \rho_g u_g^2$ much overcomes the capillary force $\propto h/\sigma$, coinciding with $We_h \gg 10^0$. Moreover, we notice that $\xi \propto \rho_g^{5/24}$ and $We_h \propto \rho_g^{5/8}$, providing the clear relation of $\xi \propto We_h^{1/3}$. Validity of the present model convinces the comprehensive scenario leading to the entrainment, consist of every intermediate step that the liquid film is three-dimensionally corrugated by the two types of instabilities (KH and RT) driven by the turbulent gas stream, followed by the formation of cusps as the origin of entrainment.

B. Evaporating Film

We analyze two types of combustion tests for bipropellant thrusters with distinct thrust levels, denoted in Table 2. The oxidizer is mixture of nitrogen tetroxide with 3% nitric oxide (MON3), while the fuel is monomethylhydrazine (MMH) for the 10N thruster and hydrazine for the 500N thruster, respectively. The chamber configurations are equivalent to the flight models. For the 10N case, the chamber is made of quartz glass to visualize the internal dynamics of liquid film. Based on the verified stratified stream tube assumption for the combustion gas flow inside rocket engines[21, 43], the self-decomposing gas of liquid film covers the liquid film surface; thus, we use T_c as the self-decomposing temperature of the fuel. Nominal conditions providing Q and ρ_g are $M_R = 1.6$ in the 10N case and $P_c = 1$MPa in the 500N case. The flow rate ratio of Q to the overall fuel is set to approximately 0.3 via the area of the film injection orifices and the fuel injectors. The gas velocity of u_g is obtained by the mass conservation between the injected propellants and gas stream at all the propellants becoming gas phase inside the combustion chamber. For rocket engines in general, it is known that $Q \propto P_c$ and $\rho_g \propto P_c$. Reliability of the experimental data is previously confirmed[3].

Figure 5 depicts the experimental results for wavy liquid films in the 10N thruster with the present theoretical results. The visualization image in Fig. 5(a) uncovers internal dynamics of the coolant liquid film with the accompanying fast combustion gas stream. The liquid film is not smooth at all, clearly spreading with the complex wavy pattern. In Fig. 5(b), the calculated results well coincide with the experimental results, reproducing $u_m \approx 1\text{m/s}$ and $h \sim 10\mu\text{m}$ in the range of mixture ratio. The film Reynolds number is consistently $Re_l \sim O(10^1)$. As the mixture ratio increases, the film flow rate decreases, leading to slightly thinner film at the large M_R conditions. Fuel jets impinge on the chamber inner surface for producing the film with the ejection velocity over 10m/s, much faster than the film velocity, indicating that the initial inertia of the film promptly diminishes by the wall friction and the film is driven sheared by the gas stream, consistent with the experimental observations[3]. The measured axial wavelength in Fig. 5(c) is $\lambda \approx 1\text{mm}$. Overestimation by the theoretical result may be attributed to the difficulty of measuring the individual axial wavelength on three-dimensionally corrugated film inside the glass chamber. The order of magnitude, however, can be captured by the present analysis.

Table 2 Combustion test conditions

Nominal thrust	10N[3]	500N
Coolant fuel	MMH	Hydrazine
Chamber	Glass	Ceramic
D[mm]	10	50
M_R	1.0/1.6/2.1	0.8
T_c[K]	1000	850
P_c[MPa]	1	0.5~1
Nominal Q[ml/s]	1	50
Nominal ρ_g[kg/m^3]	1.3	1.3
u_g[m/s]	100	200
η_g[μPa·s]	30	30
ρ_l[kg/m^3]	870	1010
η_l[mPa·s]	0.8	1
σ[mN/m]	34	67
ΔH[MJ/kg]	0.88	1.4
T_s[K]	360	450

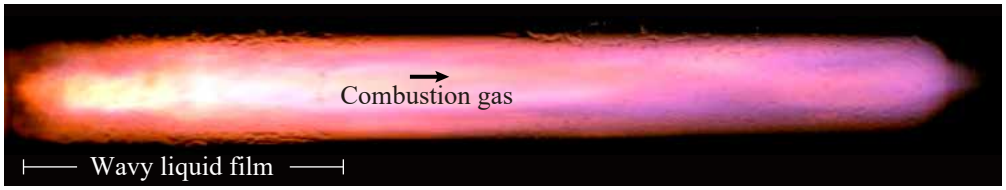

(a) Self-luminous instantaneous image at M_R = 1.6.

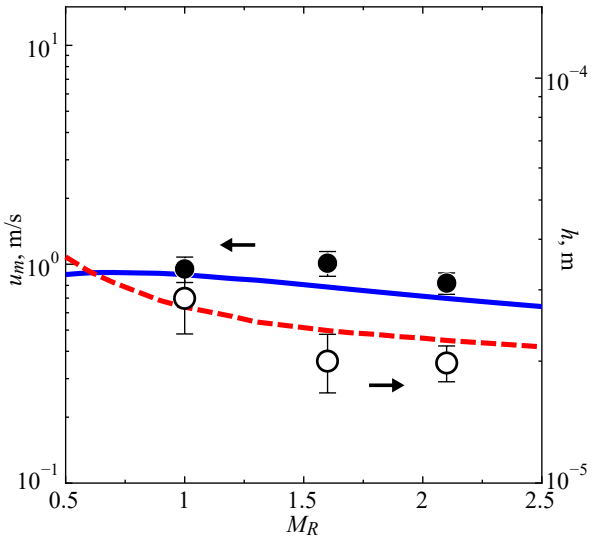

(b) Velocity and thickness.

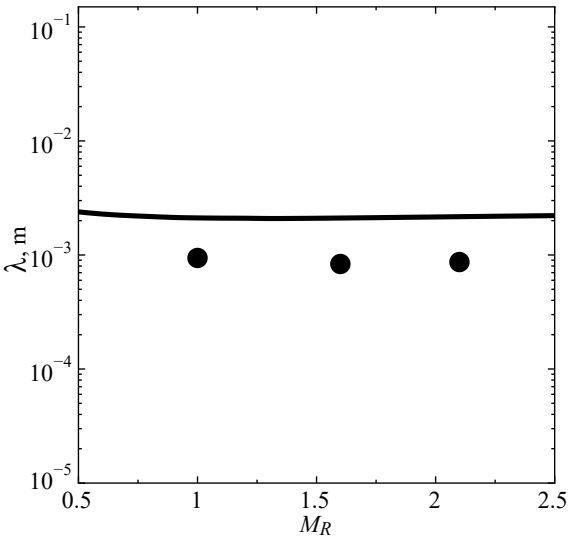

(c) Axial wavelength.

Fig. 5 Wavy film characters against mixture ratio in 10N case.
(b)(c)Symbols are experimental results, and lines are calculated results. Error bars indicate standard error.

Figure 6 presents the theoretical results of wavy liquid film characters against combustion pressure for the conditions of 500N thruster. In Fig. 6(a), as P_c increases, the film becomes faster and thicker. Substituting relationships of $Re_l \propto Q \propto P_c$ and $Re_g \propto \rho_g \propto P_c$ into Eqs. (5)(6), we deduce $u_m \propto P_c^{7/8}$ and $h \propto P_c^{1/8}$, denoting that u_m is more sensitive to P_c. In Fig. 6(b), the instabilities are enhanced according to the increment of P_c. The vorticity thickness thins following $\delta \propto P_c^{-3/4}$ in Eq. (7), leading to $\lambda \propto P_c^{-5/4}$ and $\lambda_p \propto P_c^{-7/6}$. The ratio is, however, almost constant as $\lambda_p/\lambda \propto P_c^{1/12}$, weakly dependent on P_c. Using those wavy film characters, we calculate entrainment rate against P_c as in Fig. 7(a). Although the absolute amount of entrainment increases as P_c increases accordingly, the ratio to $Q(\propto P_c)$ decreases. Here, the reduction of effective coolant flow rate up to 40 % is quantitatively confirmed due to the droplet entrainment detached from the film. From Eq. (9), we notice $u_c \propto P_c^{0.5}$; thus, the velocity ratio varies $u_c/u_m \propto P_c^{-3/8}$. Combining with $\lambda_p/\lambda \propto P_c^{1/12}$, we obtain $\xi \propto P_c^{-7/24}$. We emphasize that the deterioration of film cooling performance by entrainment becomes mitigated at higher combustion pressure. Simultaneously, the wavy film can expand the wet area exposed to the combustion gas, shown in Fig. 7(b). At P_c < 0.5 MPa, however, both wavelengths, λ and λ_p, are sufficiently longer than h ($\lambda_p/h \gg 10^0$), indicating that the liquid film can be regarded as smooth or a long wave condition. As P_c increases typically at P_c > 0.5 MPa, h slightly thickens and λ_p shortens, the ripple wave dominantly contributes to the increment of χ. Assuming that h/λ_p becomes enough large at $P_c \approx$ 1MPa, we deduce $\chi \approx \chi_p \sim h/\lambda_p \propto P_c^{31/24}$. The roll wave will enlarge the wet area at much higher combustion pressure conditions, *e.g.* $P_c \sim$ 10MPa, in addition to the ripple wave.

Incorporating the reduction of film flow rate by the entrainment and promotion of heat transfer by the wavy film structure, we finally analyze the coolant film length by Eq. (13), normalized by the chamber length of $L_c \approx$ 100mm.

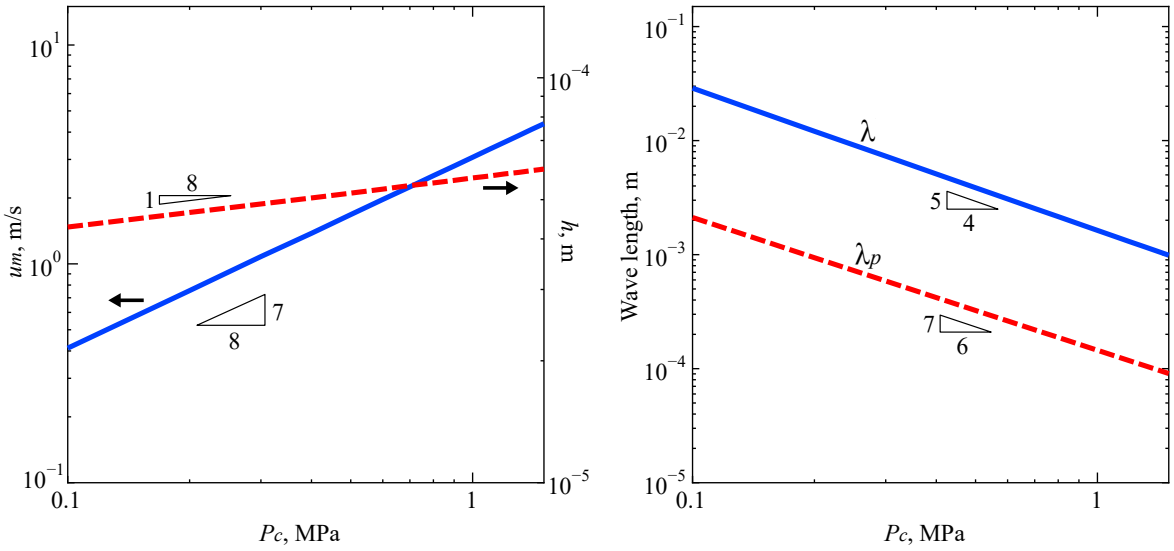

(a) Velocity and thickness.

(b) Instability wavelengths.

Fig. 6 Wavy film characters against combustion pressure in 500N case.

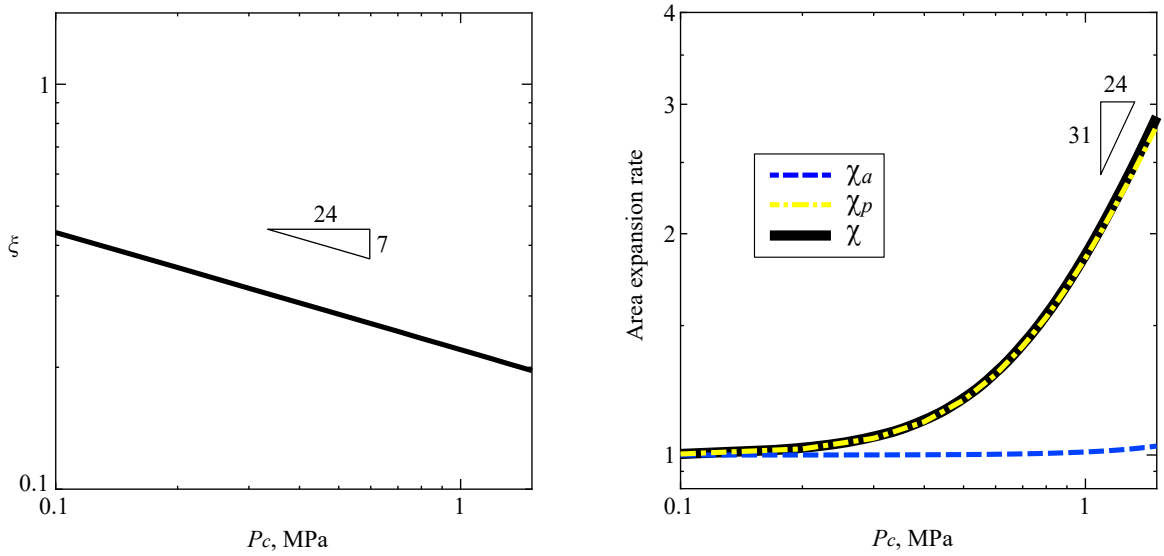

(a) Entrainment rate.

(b) Area expansion rate.

Fig. 7 Film characters with entrainment and corrugation in 500N case.

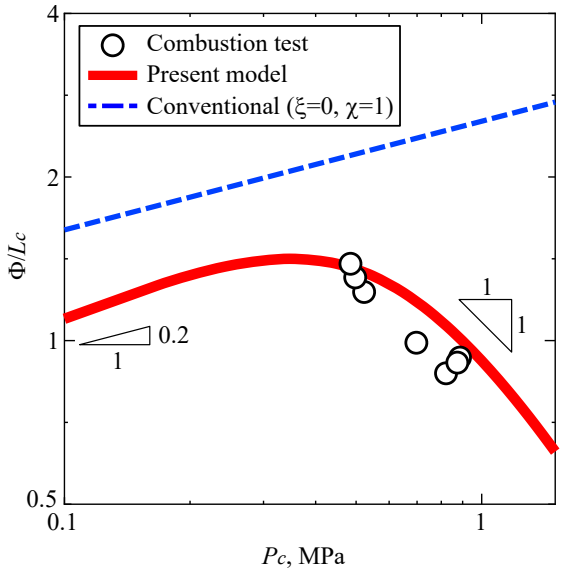

Fig. 8 Film cooling length in 500N case.

Identification of the film length is declared in Appendix A. Figure 8 demonstrates that the calculated result of film length based on the present model well reproduces the combustion test results, in which the film length shortens as the increment of P_c, evidencing the validity of the present model for the evaporating liquid film. At the small P_c condition, it was confirmed $\chi \approx 1$ in Fig. 7(b). The entrainment is not negligible as a bias, leading to the net flow rate of the liquid film being $Q(1-\xi) \underline{\propto} P_c$. At $P_c \approx 0.1$MPa, we obtain

$$\Phi \underline{\propto} P_c^{0.2}. \tag{14}$$

Reaching $P_c \approx 1$MPa, we deduce following relation by substituting $\chi \propto P_c^{31/24}$,

$$\Phi \propto P_c^{-131/120} \underline{\propto} P_c^{-1}. \tag{15}$$

The drastic change of film length from elongation to shortening around $P_c \approx 0.5$MPa is now revealed, attributed to the expanding wetting area, enlarging along the circumferential direction in particular, not to the entrainment. The good agreement also indicates that the heat transfer between the combustion gas (decomposing fuel gas) and the liquid film is the primary factor determining the film length, and the heat conduction from the chamber wall, partially heats the liquid film front below, is subdominant. The radiation heat transfer from the combustion gas to the liquid film is insignificant at the present conditions. The adiabatic wall is again convinced as a reasonable boundary condition[39]. On the contrary, the conventional model shows the film continuously elongates, being proportional to ${P_c}^{0.2}$, because the effect of coolant flow rate $Q \propto P_c$ overcomes the heat flux $\propto h_g \propto P_c^{0.8}$, depicting a completely opposite trend to the combustion test results. Therefore, it is clearly demonstrated that the 3D liquid film dynamics are the essential factor for the accurate prediction of evaporating coolant film length. 2D assumption and/or the enhancing heat transfer just following $h_g \propto P_c^{0.8}$ are insufficient.

IV. Conclusion

Evaporating liquid film dynamics sheared by turbulent gas flows are theoretically investigated as a general thermo-fluid issue. We successfully implement two important factors of 3D wavy structure and droplet entrainment, allowing for deriving the original formulation for the film length or dryout point. The fate of evaporating liquid film follows the scenario that the turbulent gas flow soon drives the liquid film being Couette flow, the velocity gap between the film and gas initiates the Kelvin-Helmholtz instability along the axial direction followed by the Rayleigh-Taylor instability along the transverse direction, the superposition of the two instabilities creates cusps on the film as the origin of entrainment, and the convective heat transfer from the hot gas eventually evaporates the liquid film. The entrainment reduces the net film flow rate. Simultaneously, the cusps enlarge the area of liquid/gas interface. The combustion tests for the bipropellant thrusters present a typical trend that the coolant film length shortens approximately inversely proportional to the combustion pressure, well reproduced by the present modeling framework combining with Bartz equation. It is emphasized that effect of wet area expansion is the primary factor for promoting the heat transfer at high combustion pressure conditions, overcoming other factors of entrainment and increment of heat transfer coefficient. The physically-consistent comprehensive model clearly convinces us that the 3D film architecture is essential for the accurate prediction of evaporating liquid film dynamics.

Appendix: Definition of Film Length

In the 500N case, the distribution of temperature on outer surface of the combustion chamber set in a vacuum chamber was measured by using an infrared camera through germanium glass window after reaching a steady state as in Fig. 9(a). An experimental result of the circumferentially averaged temperature of T is shown in Fig. 9(b). We calculate the temperature gradient along the axial direction by dT/dx, identifying the position corresponding to the maximum value as the film length of Φ. The temperature in the region fully covered by the coolant film, $x < \Phi$, is confirmed being almost equivalent with the saturation temperature of the fuel, again convincing the validity of adiabatic boundary condition for the internal film flow. Once the film dries, the temperature rapidly increases, reaching the maximum temperature close to the throat and gradually decreasing downstream.

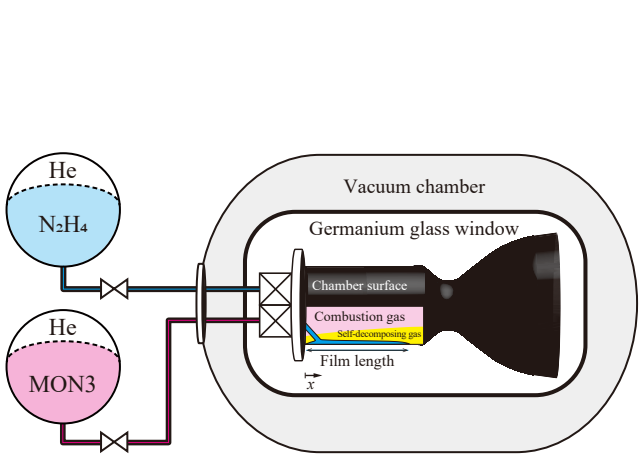

(a) Schematics of the experimental setup.

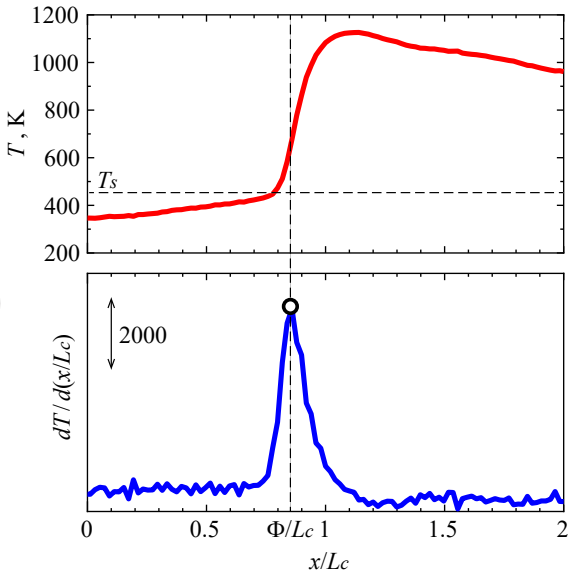

(b) Temperature distribution on outer surface of the combustion chamber to determine the film length.

Fig. 9 Combustion test for the 500N bipropellant thruster.

Acknowledgments

This study was supported by JSPS KAKENHI, JP21H01251.

References

[1] Shine, S., and Nidhi, S., "Review on Film Cooling of Liquid Rocket Engines," *Propulsion Power Research.*, Vol. 7, No. 1, 2018, pp. 1–18. DOI:10.1016/j.jppr.2018.01.004.

[2] Yuan, C., Li, J., Jiang, Z., and Yu, H., "Experimental Investigation of Liquid Film Cooling in Hypersonic Flow," *Physics of Fluids*, Vol. 31, 2019, p. 046101. DOI:10.1063/1.5088024.

[3] Fujii, G., Daimon, Y., Furukawa, K., Inoue, C., Shiraiwa, D., and Tanaka, N., "Visualization of Coolant Liquid Film Dynamics in Hypergolic Bipropellant Thruster," *Journal of Propulsion and Power*, 2021. DOI:10.2514/1.B38421.

[4] Baumert, A., Bansmer, S., Trontin, P., and Villedieu, P., "Experimental and Numerical Investigations on Aircraft Icing at Mixed Phase Conditions," *International Journal of Heat and Mass Transfer*, Vol. 123, 2018, pp. 957–978. DOI:10.1016/j.ijheatmasstransfer.2018.02.008.

[5] Shinan, C., Weidong, Y., Mengjie, S., Mengyao, L., and Qiyu, S., "Investigation on Wavy Characteristics of Shear-Driven Water Film Using the Planar Laser Induced Fluorescence Method," *International Journal of Multiphase Flow*, Vol. 118, 2019, pp. 242–253. DOI:10.1016/j.ijmultiphaseflow.2019.04.016.

[6] Chen, N., Hu, Y., Ji, H., and Zhang, M., "Hot-Air Anti-Icing Heat Transfer and Surface Temperature Modeling," *AIAA Journal*, Vol. 59, No. 9, 2021, pp. 3657–3666. DOI:10.2514/1.J059776.

[7] Kuznetsov, V., and Fominykh, E., "Evaporation of a Liquid Film in a Microchannel Under the Action of a Co-Current Dry Gas Flow," *Microgravity Science and Technology*, Vol. 32, 2020, pp. 245–258. DOI:10.1007/s12217-019-09765-z.

[8] Ishii, M., and Grolmes, M. A., "Inception Criteria for Droplet Entrainment in Two-Phase Concurrent Film Flow," *AIChE Journal*, Vol. 21, No. 2, 1975, pp. 308–318. DOI:10.1002/aic.690210212.

[9] Marmottant, P., and Villermaux, E., "On Spray Formation," *Journal of Fluid Mechanics*, Vol. 498, 2004, pp. 73–111. DOI:10.1017/S0022112003006529.

[10] Cherdantsev, A. V., Hann, D. B., and Azzopardi, B. J., "Study of Gas-Sheared Liquid Film in Horizontal Rectangular Duct Using High-Speed LIF Technique: Three-Dimensional Wavy Structure and Its Relation to Liquid Entrainment," *International Journal of Multiphase Flow*, Vol. 67, 2014, pp. 52–64. DOI:10.1016/j.ijmultiphaseflow.2014.08.003.

[11] Pham, S. H., Kawara, Z., Yokomine, T., and Kunugi, T., "Detailed Observations of Wavy Interface Behaviors of Annular Two-Phase Flow on Rod Bundle Geometry," *International Journal of Multiphase Flow*, Vol. 59, 2014, pp. 135–144. DOI:10.1016/j.ijmultiphaseflow.2013.11.004.

[12] Cherdantsev, A., Hann, D., Hewakandamby, B., and Azzopardi, B., "Study of the Impacts of Droplets Deposited from the Gas Core onto a Gas-Sheared Liquid Film," *International Journal of Multiphase Flow*, Vol. 68, 2017, pp. 69–86. DOI:10.1016/j.ijmultiphaseflow.2016.09.015.

[13] Issa, S., and Macian-Juan, R., "Droplets Entrainment Ratio in a PWR Hot-Leg Pipe Geometry," *Nuclear Engineering and Design*, Vol. 330, 2018, pp. 1–13. DOI:10.1016/j.nucengdes.2018.01.010.

[14] Yarygin, V., Prikhodko, V., Yarygin, I., and Vyazov, Y., "Near-Wall Liquid Film Interaction with Co-Current Gas Flow Inside Nozzle and Under Outflow into Vacuum," *Vacuum*, Vol. 159, 2019, pp. 494–499. DOI:10.1016/j.vacuum.2018.11.002.

[15] Inoue, C., and Maeda, I., "On the Droplet Entrainment from Gas-Sheared Liquid Film," *Physics of Fluids*, Vol. 33, No. 1, 2021, p. 011705. DOI:10.1063/5.0038399.

[16] Vollestad, P., Ayati, A., and Jensen, A., "Microscale Wave Breaking in Stratified Air-Water Pipe Flow," *Physics of Fluids*, Vol. 31, 2019, p. 032101. DOI:10.1063/1.5082607.

[17] Cherdantsev, A., "Overview of Physical Models of Liquid Entrainment in Annular Gas-Liquid Flow," *AIP Conference Proceedings*, Vol. 1939, 2018, p. 020006. DOI:10.1063/1.5027318.

[18] Berna, C., Escrivá, A., Muñoz-Cobo, J., and Herranz, L., "Review of Droplet Entrainment in Annular Flow: Interfacial Waves and Onset of Entrainment," *Progress in Nuclear Energy*, Vol. 74, 2014, pp. 14–43. DOI:10.1016/j.pnucene.2014.01.018.

[19] Stechman, R., Oberstone, J., and Howell, J., "Design Criteria for Film Cooling for Small Liquid Propellant Rocket Engines," *Journal of Spacecraft and Rockets*, Vol. 6, 1969, pp. 97–102. DOI:10.2514/3.29545.

[20] Fujii, G., Daimon, Y., Inoue, C., Shiraiwa, D., Tanaka, N., and Furukawa, K., "Visualization of Pulse Firing Mode in Hypergolic Bipropellant Thruster," *Journal of Propulsion and Power*, Vol. 36, No. 5, 2020, pp. 677–684. DOI:10.2514/1.B37637.

[21] Inoue, C., Oishi, Y., Daimon, Y., Fujii, G., and Kawatsu, K., "Direct Formulation of Bipropellant Thruster Performance for Quantitative Cold-Flow Diagnostic," *Journal of Propulsion and Power*, 2021. DOI:10.2514/1.B38310.

[22] Kinney, G., Abramson, A., and J.L.Sloop, "Internal Liquid Film Cooling Experiments with Air Stream Temperatures to 2000F in 2 and 4 Inch Diameter Horizontal Tubes," *National Advisory Committee for Aeronautics Report*, Vol. TR-1087, 1952, pp. 1–21.

[23] Morrell, G., "Investigation of Internal Film Cooling of 1000 Pound Thrust Liquid Ammonia-Liquid Oxygen Rocket Engine Combustion Chamber," *NACA*, Vol. RM E51E04, 1951, pp. 1–42.

[24] Arnold, R., Suslov, D., and Haidnn, O., "Experimental Investigation of Film Cooling with Tangential Slot Injection in a LOX/CH4 Subscale Rocket Combustion Chamber," *Transactions of the Japan society for aeronautical and space sciences*, Vol. 7, 2009, pp. 81–86. DOI:10.2322/tstj.7.Pa$_8$1.

[25] Crocco, L., "An Approximate Theory of Porous, Sweat, or Film Cooling With Reactive Fluids," *Journal of the American Rocket Society*, Vol. 22, No. 6, 1952, pp. 331–338. DOI:10.2514/8.4508.

[26] Arnold, R., Suslov, D., and Haidn, O., "Film Cooling of Accelerated Flow in a Subscale Combustion Chamber," *Journal of Propulsion and Power*, Vol. 25, 2009, pp. 443–451. DOI:10.2514/1.39308.

[27] Shine, S., Kumar, S., and Suresh, B., "A New Generalized Model for Liquid Film Cooling in Rocket Combustion Chamber," *International Journal of Heat and Mass Transfer*, Vol. 55, 2012, pp. 5065–5075. DOI:10.1016/j.ijheatmasstransfer.2012.05.006.

[28] Jand, D., Kwak, Y., and Kwon, S., "Design and Validation of a Liquid Film-Cooled Hydrogen Peroxide/Kerosene Bipropellant Thruster," *Journal of Propulsion and Power*, Vol. 31, 2015, pp. 761–765. DOI:10.2514/1.B35434.

[29] Ma, X., Wang, Y., and Tian, W., "A Novel Model of Liquid Film Flow and Evaporation for Thermal Protection to a Chamber with High Temperature and High Shear Force," *International Journal of Thermal Sciences*, Vol. 172, 2022, p. 107300. DOI:10.1016/j.ijthermalsci.2021.107300.

[30] Nikuradse, J., "Gesetzmassigkeiten der Turbulenten Stromung in Glatten Rohren," *Forschung auf dem Gebiet des Ingenieurwesens A*, Vol. 4, 1932, p. 44. DOI:10.1007/BF02716946.

[31] Moody, L., "Friction Factors for Pipe Flow," *Transactions of the American Society of Mechanical Engineers*, Vol. 66, 1944, pp. 671–684.

[32] Schlichiting, H., "Boundary Layer Theory," *McGaw-Hill Seri. Mech. Eng.*, 1968.

[33] Himmelsbach, J., Noll, B., and Witting, S., "Experimental and Numerical Studies of Evaporating Wavy Fuel Films in Turbulent Air Flow," *International Journal of Heat and Mass Transfer*, Vol. 37, No. 8, 1994, pp. 1217–1226. DOI:10.1016/0017-9310(94)90207-0.

[34] Rayleigh, L., "On the Stability, or Instability, of Certain Fluid Motions," *Proceedings of the London Mathematical Society*, Vol. 11, No. 1, 1880, pp. 57–72. DOI:10.1112/plms/s1-11.1.57.

[35] Villermaux, E., "On the Role of Viscosity in Shear Instabilities," *Physics of Fluids*, Vol. 10, 1998, pp. 368–373. DOI:10.1063/1.869529.

[36] Dimotakis, P., "Two-Dimensional Shear-Layer Entrainment," *AIAA Journal*, Vol. 24, No. 11, 1986, pp. 1791–1796. DOI:10.2514/3.9525.

[37] Rayleigh, L., "Investigation of the Character of the Equilibrium of an Incompressible Heavy Fluid of Variable Density," *Proceedings of the London Mathematical Society*, Vol. 14, No. 1, 1883, pp. 170–177. DOI:10.1112/plms/s1-14.1.170.

[38] Taylor, G., "The Instability of Liquid Surfaces when Accelerated in a Direction Perpendicular to their Planes. I," *Proceedings of The Royal Society A*, Vol. 201, 1950, pp. 192–196. DOI:10.1098/rspa.1950.0052.

[39] Collier, J., and Thome, J., *Convective Boiling and Condensation*, 3rd ed., Clarendon Press, Oxford, 1996, Chap. 7.

[40] Bartz, D., "A Simple Equation for Rapid Estimation of Rocket Nozzle Convective Heat Transfer Coefficients," *Jet Propulsion*, Vol. 27, No. 1, 1957, pp. 49–53. DOI:10.2514/8.12572.

[41] McAdams, W., *Heat Transmission*, 2nd ed., McGraw-Hill, New York, 1942, Chap. 3.

[42] Winterton, R., "Where did the Dittus and Boelter equation come from?" *International Journal of Heat and Mass Transfer*, Vol. 41, No. 4-5, 1998, pp. 809–810. DOI:10.1016/S0017-9310(97)00177-4.

[43] Wrobel, J. R., "Some Effects of Gas Stratification on Choked Nozzle Flows," *Journal of Spacecraft and Rockets*, Vol. 2, No. 6, 1965, pp. 918–922. DOI:10.2514/3.28314.

[44] Leng, M., Chang, S., and Wu, H., "Experimental Investigation of Shear-Driven Water Film Flows on Horizontal Metal Plate," *Experimental Thermal and Fluid Science*, Vol. 94, 2018, pp. 134–147. DOI:10.1016/j.expthermflusci.2018.02.004.